AIDIC *Conference Series*, Vol. 10, 2011
Editor Sauro Pierucci
DOI: 10.3303/ACOS1110038
ISBN 978-88-95608-58-7 ISSN 2036-5969

INFLUENCE OF CRYOMILLING ON SPARK PLASMA SINTERING OF CoNiCrAlY POWDERS

Sara Todde[1], Roberta Licheri[1], Selena Montinaro[2], Roberto Orrù[1,*], Giacomo Cao[1,2,*]

[1]Dipartimento di Ingegneria Chimica e Materiali, Unità di Ricerca del Consorzio Interuniversitario Nazionale per la Scienza e Tecnologia dei Materiali (INSTM), Unità di Ricerca del Consiglio Nazionale delle Ricerche (CNR) – Dipartimento di Energia e Trasporti, Università degli Studi di Cagliari, Piazza D'Armi, 09123 Cagliari, Italy, Email: orru@dicm.unica.it, cao@dicm.unica.it
[2]Centro Interdipartimentale di Ingegneria e Scienze Ambientali (CINSA) and Laboratorio di Cagliari del Consorzio Interuniversitario Nazionale la Chimica per l'Ambiente (INCA), via S. Giorgio 12, 09124 Cagliari, Italy

The characteristics of Co-32Ni-21Cr-8Al-0.5Y (wt. %) cryomilled powders are systematically examined in this work as a function of the cryogenic treatment conditions adopted, specifically milling time and ball to powders weight ratio. Morphology changes, particle size increase, crystallite size decrease down to nanometric level and the formation of oxide nanodispersoids are the main consequences produced in the processed powders. These features are found to be responsible for the significant influence of powders cryomilling on their Spark Plasma Sintering (SPS) behaviour. In particular, sintering is progressively promoted until cryomilling intensity does not overcome a certain level while densification becomes relatively more difficult with severely cryomilled powders. A significant microstructure refinement is obtained in SPSed samples when cryomilled powders are used. Moreover, an α-Al_2O_3 layer tends to be exclusively produced on the external surface of cryomilled specimens oxidized at 1100°C, thus limiting the presence of less protective mixed oxides, otherwise formed in unmilled samples. The higher protective character of the oxide layer is evidenced by the fact that Al depletion from the bulk of the CoNiCrAlY alloy is correspondingly reduced. This is an important outcome for the improvement of high-temperature oxidation resistance in thermal barrier coatings of gas turbine engines.

1. INTRODUCTION

To withstand the severe oxidation conditions encountered during their utilization, Ni-superalloys-based gas turbine components are typically protected with thermal barrier coatings (TBC), where the bond-coat layer is based on MCrAlY alloys (M=Ni, Co) (Sahoo et al., 1998). In this regard, in order to prevent the progress of internal oxidation under such conditions, it is well established that a dense and continuous oxide layer mainly consisting of α-Al_2O_3 (cf. Fig. 1) has to be formed on the MCrAlY bond coat surface that is in contact with the yttria stabilized zirconia top coat of the TBC (Tang et al., 2004; Young, 2008).

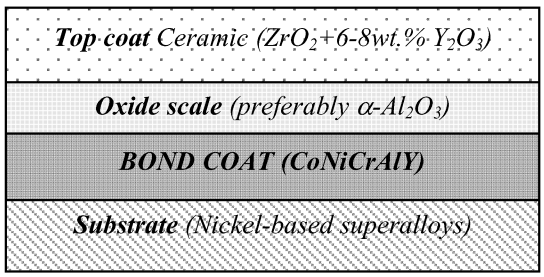

Fig. 1: Schematic representation of the layers present in a Thermal Barrier Coating (TBC).

Please cite this article as: Todde S., Licheri R., Montinaro S., Orru R. and Cao G., (2011), Influence of cryomilling on spark plasma sintering of conicraly powders, AIDIC Conference Series, 10, 343-352 DOI: 10.3303/ACOS1110038

Several investigations have been recently conducted with the aim of improving high temperature oxidation resistance properties of MCrAlY alloys, so that the operating temperature could be increased and/or the service life of TBC extended (Tang et al., 2004; Young, 2008; Ma and Schoenung, 2010). In this context, beneficial effects are observed when decreasing grain size in bond coat metal matrix and/or in presence of nano-sized dispersions of hard phases such as oxides, nitrides, etc. (Tang et al., 2004). Moreover, the presence of oxide dispersoids was found to produce a strengthening effect in MCrAlY materials (Witkin and Lavernia, 2006).
One possible approach for obtaining both grain size refinement in metal matrix and the formation of nanosized ceramic dispersoids is represented by cryomilling, consisting in ball- or attrition-milling of conventional raw powders in a cryogenic medium, typically nitrogen (Witkin and Lavernia, 2006; Lavernia et al., 2008). Cold-welding, continuous defect generation, fracturing phenomena, comminution, nanometric refinement of microstructure, extension of solid solubility limits, synthesis of novel crystalline and amorphous phases, etc., are the well recognized typical features taking place during milling processes (Suryanarayana, 2001). The most significant operating parameters influencing the milling treatment are the charge ratio (CR) or ball to powder mass ratio, milling time and rotational speed. Nevertheless, other variables such as milling device, atmosphere, process control agents, etc., may also affect the characteristics of the resulting powders.
As compared to conventional room-temperature milling, processes conducted under cryogenic conditions are more effective with the aim of obtaining nanostructured materials, since recovery and recrystallization phenomena are restrained at lower temperatures thus leading to a more rapid grain size refinement (Suryanarayana, 2001).
The efficacy of cryogenic treatment on TBC properties can be assessed, in principle, only after spraying the cryomilled powders to produce the bond coat, but long processing times and large amount of powders are required for optimising such procedure. In this regard, the use of the SPS technology, which belong to the more general class of Electric Current Activated Sintering (ECAS) methods (Orrù et al., 2009) provides a possible efficient tool for the rapid and relatively simple production of samples to be preliminarily tested, before powder spaying to generate the complete TBC. Specifically, during SPS, electrically conductive powders are pressed uniaxially and simultaneously crossed by an electric pulsed current to produce high local heating rates due to Joule effect.
Along these lines, CoNiCrAlY- and NiCrAlY- based unmilled (Oquab et al., 2007; Ratel et al., 2010; Song et al., 2010) or NiCrAlY cryomilled powders (Ajdelsztajn et al., 2002) have been recently consolidated taking advantage of the SPS technique. Although further detailed studies are required to better understand the phenomena involved and optimising process conditions, the reported results indicate that the combination of cryomilling and SPS processes represents a promising approach for providing quick answers regarding possible benefits deriving from the cryogenic treatment.
Other than allowing the measurement of mechanical properties on dense samples, otherwise difficult on MCrAlY bond coats, the use of SPS processes is particularly time- and cost-saving for the preliminary evaluation of oxidation resistance properties under different cryomilling conditions, since the obtainment of the coating through spraying is not required.
The influence of ball to powder mass ratio and cryomilling time on the characteristics (morphology, particle size, composition, microstructure) of CoNiCrAlY cryomilled powders is investigated for the first time in this work. After receiving the cryogenic treatment, the obtained powders are then consolidated by SPS at different sintering temperatures to identify, depending upon the set of cryomilling parameters, the optimal conditions sufficient to achieve the complete densification of the material. The fully dense optimal products are then characterized (in terms of microstructure and oxidation resistance) and the results compared with those related to unmilled powders.

2. EXPERIMENTAL MATERIALS AND METHODS

The CoNiCrAlY powders (Sulzer Metco, Europe GmbH) used as starting materials in the present investigation have been prepared by gas atomization with nominal composition Co-32Ni-21Cr-8Al-0.5Y (wt.%) and particle size in the range of 15-45 μm. The modified attritor mill (Union Process model 01-HDDM/01-HD) shown in Fig. 2 was utilized for the mechanical treatment in liquid N_2 environment using stainless-steel balls (2 mm diameter). The influence of cryomilling time, t_{CR} was investigated in the range of 0-12 h, the charge ratio, CR

was changed from 4 to 30 while the rotation speed of the attritor impeller, R, was maintained equal to 600 rpm during all experiments.
The SPS apparatus (mod. 515S, Sumitomo Heavy Industries Ltd., Japan) displayed in Fig. 3 was used under vacuum (10 Pa) and in the temperature controlled mode for consolidating either as-received or cryomilled powders. This equipment mainly consists of a power supply (DC-pulse generator), to provide a maximum current and voltage equal to 1500 A and 10 V, respectively, and an uniaxial press able to produce mechanical loads in the range 3-50 kN. The power supply generates current pulses of 3.3 ms fixed duration and the 12/2 on/off pulse sequence was adopted in this work.
About 4 g of MCrAlY powders to be sintered were poured into graphite dies with 30 mm outside diameter, 15 mm inside diameter, and 30 mm height. Graphite contamination from the plungers to the metal powders undergoing sintering was observed during preliminary SPS experiments. To overcome this drawback, two tantalum disks (14.7 mm diameter and 2 mm thickness) were placed between powders and plungers to provide efficient diffusion barriers for carbon. Electric current intensity and voltage are recorded in real time during the sintering process. Temperature measurements carried out using a K-type thermocouple (Omega Engineering Inc., USA) inserted in a small hole drilled on the lateral surface of the graphite die are also correspondingly provided. An indication of the product densification evolution is represented by the displacement output. However, the latter one also includes thermal expansion of sample, both electrodes, graphite blocks, spacers and plungers. All these contributions, but that of the sample, can be taken into account separately following a specific procedure reported elsewhere for the sake of brevity (Locci et al., 2006), thus obtaining the heretoafter indicated sample shrinkage (δ). For the sake of reproducibility, each experiment was repeated at least twice.
The effect of the sintering temperature, T_D was investigated in the range 750-1000 °C by performing all SPS experiments at constant values of the heating rate, 100 °C/min, mechanical pressure, P=20 MPa, and the dwell time, t_D=10 min, i.e. the time for which the system temperature is held to the T_D value.
Particle size distribution of starting and cryomilled powders was determined using a laser light scattering analyzer (CILAS 1180, France). X-ray analysis performed by a Philips PW 1830 X-rays diffractometer equipped with a Ni filtered Cu K_α radiation (λ=1.54056 Å) was used for phase identification. In addition, crystallite size evolution during cryomilling was estimated from the line broadening of X-ray diffraction peaks using the Scherrer formula (Langford and Wilson, 1978), i.e. $B=\frac{k\lambda}{L\cos\theta}$, where B is the peak width, that is inversely proportional to crystallite size (L), θ is the Bragg angle, k is the Scherrer constant which has been set equal to one, and λ is the x-ray wavelength. Scanning Electron Microscopy (SEM Hitachi, mod. S4000, Japan) coupled with Energy Dispersive Spectroscopy (EDS, Kevex Sigma 32 Probe, Noran Instruments, USA) analysis were utilized to investigate powders morphology evolution during cryomilling as well as bulk products microstructure and local phase composition. Changes in oxygen content in cryomilled products, as compared to that in original powders, were determined by using a LECO TCH-600 analyzer, according to the inert gas fusion method (ASTM E-1019).

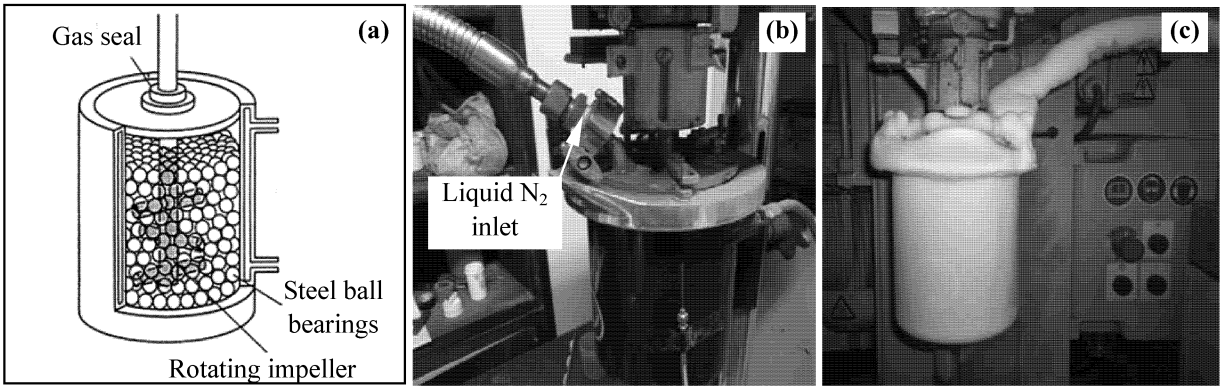

Fig. 2: Schematic representation of an attritor device (a), images of the attritor mill (Union Process model 01-HDDM/01-HD) used in the present work at room temperature (b) and under cryogenic conditions (c).

Bulk densities in SPS samples were evaluated through the Archimedes' method after accurately polishing dense products. Fully dense SPSed samples were subjected to oxidation treatment in air at 1100 °C for 20 h using a laboratory furnace (Naber-Labotherm, mod. N 50, Germany).

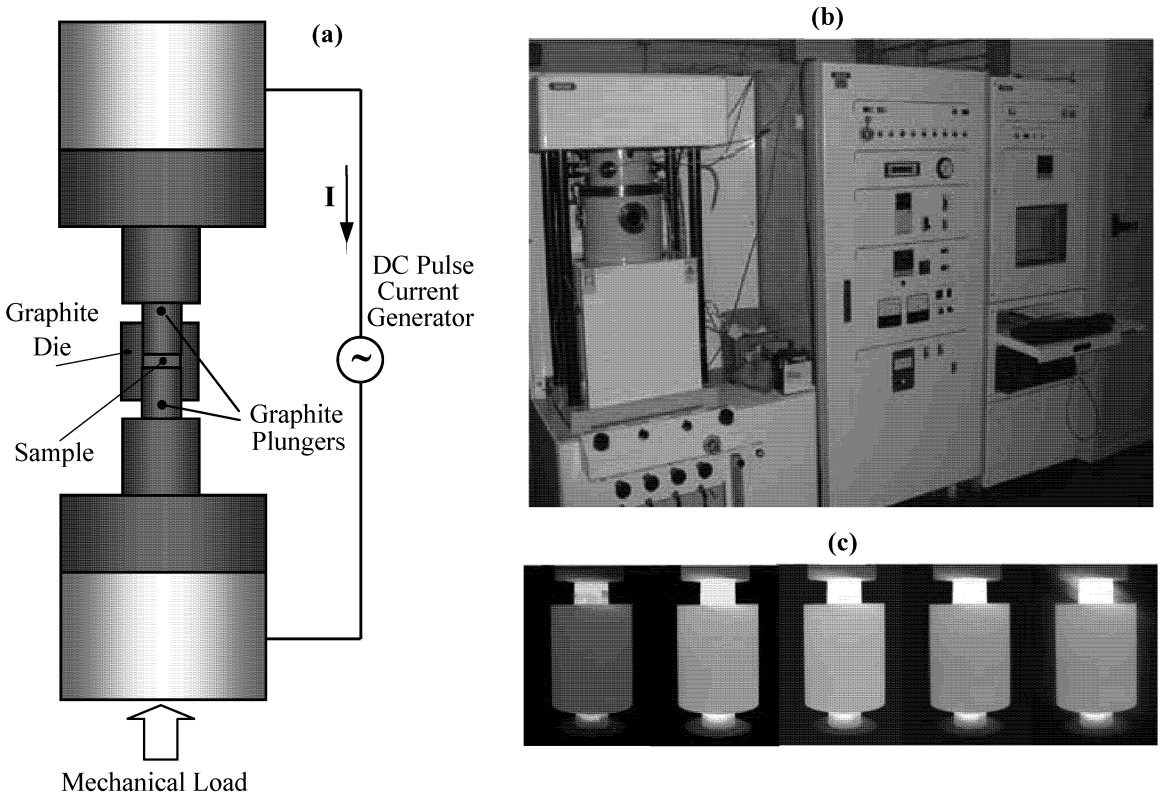

Fig. 3: Schematic representation of the SPS technique (a), general view of the SPS apparatus used in the present work (mod. 515S, Sumitomo Heavy Industries Ltd., Japan) (b) and heating/cooling sequence of the die/plungers/sample ensemble during sintering (c).

3. RESULTS AND DISCUSSION

3.1. Cryomilling

The significant changes in CoNiCrAlY powder morphology produced by the cryogenic treatment is apparent in Fig. 4(a)-4(b), where the related SEM images are shown for the cases of CR=4 and 12, respectively. The initially gas-atomized smooth and spherical particles become gradually rough, irregular and flake-like-shaped as a consequence of the cryomechanical treatment, being particle flattening enhanced at the higher CR value taken into account. In addition, a bimodal particle distribution is observed when t_{CR}= 3h and CR=30. This outcome is confirmed by particle size analysis. The presence of these two classes of powders could be associated with the heterogeneous nature of milling processes. Relatively higher deformations are induced in those particles mainly involved in mechanical actions, in this case attrition, because they are more frequently trapped between the external surfaces of milling balls, impeller and attritor wall. The percentage of powders processed under the same condition increases when milling time is augmented and, correspondingly, particles inside the attrition device tend to achieve more uniform characteristics.

The variation of the XRD patterns with cryomilling time is reported in Fig.s 5 when CR= 30. In agreement with previous findings (Tang et al., 2004), γ (CoNiCrAl, rich in Co, Ni, Cr)/γ'(Ni_3Al) and β ((Co, Ni)Al) are the only phases detected in the starting powders. As the cryomilling process proceeds, the initially sharp diffraction peaks broaden and their intensity decreases. In addition, the XRD signal corresponding to the β phase tends to disappear from the pattern. Similar observations can be made at CR=4. Crystallite size refinement and internal

strain increase induced by the milling treatment are responsible for such behaviour. The disappearance of the XRD peak related to the β phase could be either due to peaks overlap as a consequence of their broadening caused by cryomilling or the dissolution of the β phase into the γ/γ' matrix.

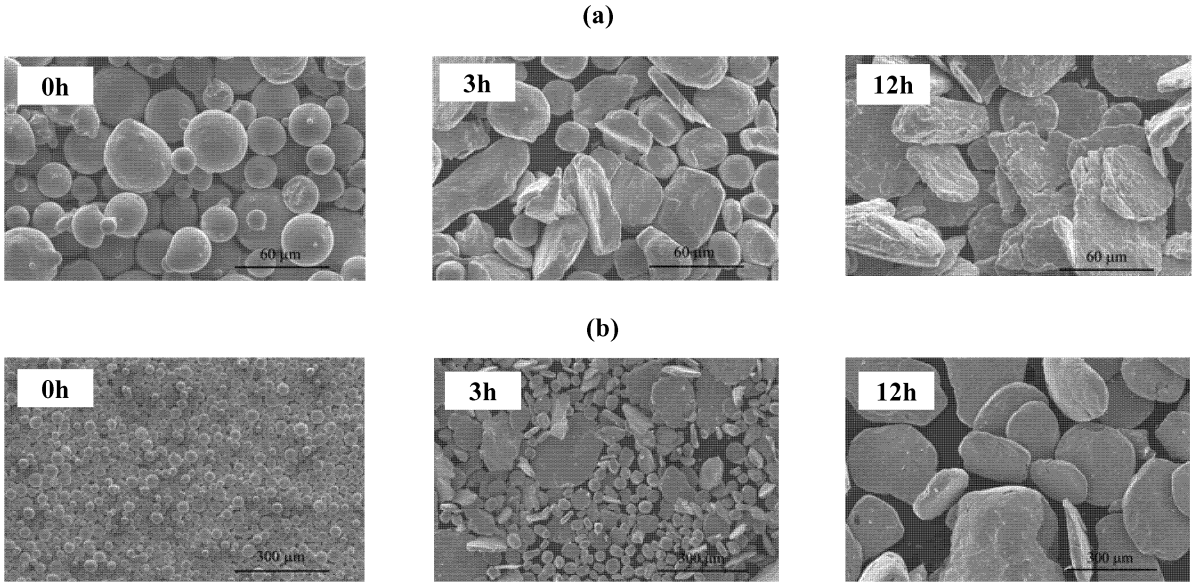

Fig. 4: Effect of cryomilling time on morphology of CoNiCrAlY powders: (a) CR=4, (b) CR=30.

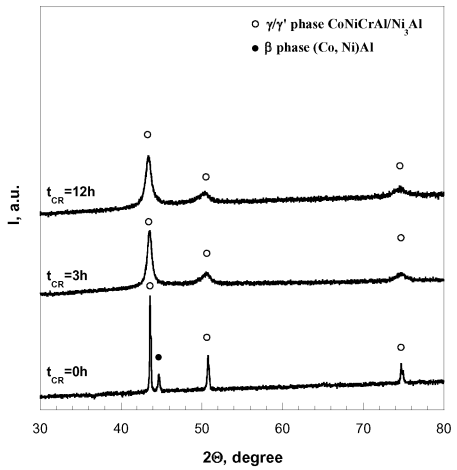

Fig. 5: XRD patterns of CoNiCrAlY powders as a function of cryomilling time (CR=30).

Some quantitative approximated values of the average crystallite size obtained under the different cryomilling conditions can be provided by the Scherrer formula. Specifically, an average crystallite size of about 15 nm is found when t_{CR}=12h and CR=30. This result is on the same order of the values reported in the literature for analogous systems processed under similar cryomilled conditions (Tang et al., 2004).
Another important feature to be accounted for is represented by possible chemical composition changes of powders which undergo the cryomilling treatment. In this regard, the oxygen content originally present in CoNiCrAlY powders, i.e. 0.04 wt.%, increases up to 0.36 wt.% when the most severe milling conditions investigated in this work are applied. This outcome, that is consistent with data reported in the literature (Tang et al., 2004), provides an indication of the formation of oxide phases, particularly Al_2O_3, during the cryomilling process.

3.2. Spark Plasma Sintering

Typical temperature and sample shrinkage (δ) measured during the SPS process, are shown in Fig. 6 for the case of dwell temperature, T_D, equal to 900 °C. In particular, the densification curves recorded when as-received and cryomilled (CR=30, t_{CR}=12 h) powders are processed under the same SPS conditions are compared. Similar modest changes in sample shrinkage are exhibited by both systems during the first 5 min after the beginning of the current application. However, densification dynamics follow a rather different behaviour as the temperature raises above 500 °C. In fact, when sintering unmilled powders, δ increases significantly only when relatively higher temperatures are achieved and the highest consolidation rate is displayed when approaching the maximum temperature. In contrast, for the case of cryomilled powders, sample consolidation is anticipated and takes place at a high, approximately constant, rate until the temperature reaches its set-point value T_D. Finally, during the isothermal stage, δ changes modestly, particularly for unmilled powders, thus reaching its final value, i.e. about 1.25 and 1.85 mm for the original and cryomilled powders, respectively, at the end of the experiment ($t=t_T$=19 min). Based on these observation, the consolidation of CoNiCrAlY powders previously cryomilled appears clearly facilitated.

The effect of sintering temperature on the relative density of bulk products obtained by SPS from powders cryomilled at different time intervals when CR=30 is reported in Fig. 7. As expected, regardless the characteristics of starting powders, sample density increases as the sintering temperature is augmented. In particular, the optimal sintering temperature required to obtain fully dense specimens when starting from as-received powders is 1000 °C. On the other hand, a non-monotonic behaviour is observed when considering the influence of the cryomilling time at CR=30. Although sintering is gradually facilitated as t_{CR} is increased up to 3h, powder consolidation becomes relatively more difficult for prolonged cryogenic treatments. Nevertheless, sintering ability of powders cryomilled for 12 h at CR=30 is higher than that exhibited by the as-received ones, consistently with the consolidation dynamics displayed by the same systems (cf. Fig. 6). On the other hand, when CR=4, it is found that powder sintering is progressively enhanced as cryomilling time is increased to 12 h.

Such behaviour can be associated to the characteristics of MCrAlY powders to be sintered. As discussed above, particle size increases, grain size refinement, internal strain increases and high defects generation represent the main effects induced by cryomilling on processing powders. While the use of larger particles makes their consolidation more difficult, grain size refinement and high defects concentration on particle surface promote sintering progress. Thus, it is possible to assess that features favouring powder consolidation overcome particles size effect, except for the case where the most severe cryomilling conditions (CR=30, t_{CR}=12 h) are adopted in our study. Another possible, complementary, role is likely played by the increase in the content of oxide dispersions in CoNiCrAlY alloy during the progress of the cryogenic treatment, since the refractory nature of these ceramics hinders powders consolidation. Unfortunately, due to their small size, in the nanometer range, the presence of these hard dispersoids cannot be directly evidenced by SEM.

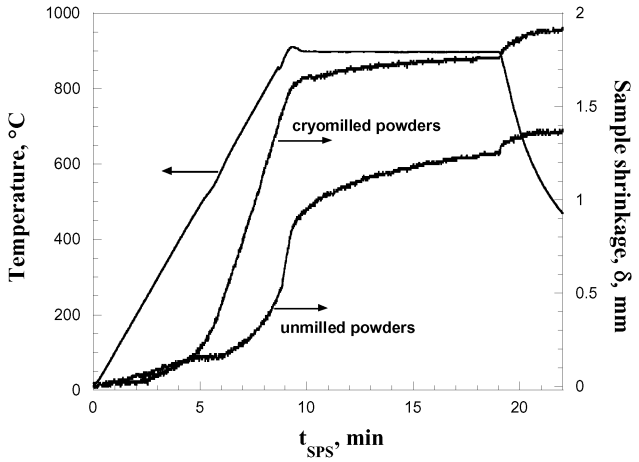

Fig. 6: Temperature and sample shrinkage temporal profiles (T_D=900 °C, 100 °C/min heating rate, t_D=10 min, P=20 MPa) during consolidation of original and cryomilled (CR=30, t_{CR}=12 h) CoNiCrAlY powders.

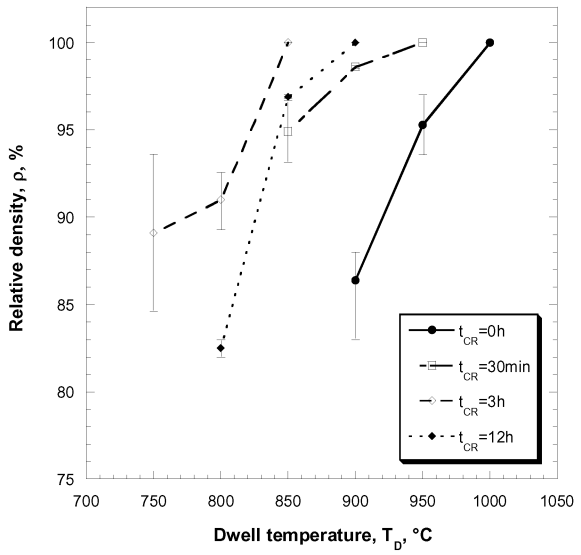

Fig.7: Influence of sintering temperature and cryomilling time on the relative density (theoretical value = 7.24 g/cm^3) of the SPSed CoNiCrAlY samples (CR=30).

Three SEM microstructures of different SPSed samples obtained when starting from original powders or after cryomilling them at CR=30 for t_{CR}=3 and 12h are compared in Fig. 8(a)-8(c), respectively. The achievement of the complete consolidation under the optimal sintering temperature identified in Fig. 7 is confirmed.
Two main regions, a darker and a lighter one, can be easily distinguished particularly in products resulting from as-received powders. Based on EDS microanalysis and taking advantage of the XRD diffraction results carried out on starting powders, it is possible to assess that the lighter continuous region contains γ/γ' phases while the darker one corresponds to the Al-rich β phase. The presence of a β + γ/γ' microstructure is consistent with previous investigations reported in the literature on the same system (Tang et al., 2004).
It is clearly seen that the relatively coarser microstructure of standard samples becomes progressively finer when a cryomilling step is carried out before sintering. In particular, two zones characterized by different microstructures can be identified throughout the samples after 3h cryomilling (cf. Fig. 8(b)). One of these region displays a microstructure similar to that obtained when densifying original powders, while the second zone is characterized by a new microstructure where the darker and lighter phases are distributed very finely in form of "stripes". Furthermore, as the cryomilling process was prolonged to 12h, the latter structure almost involves the entire CoNiCrAlY sample, as reported in Fig. 8(c). In particular, detailed observations have revealed that phase distribution is in this case at a sub-micrometer level.

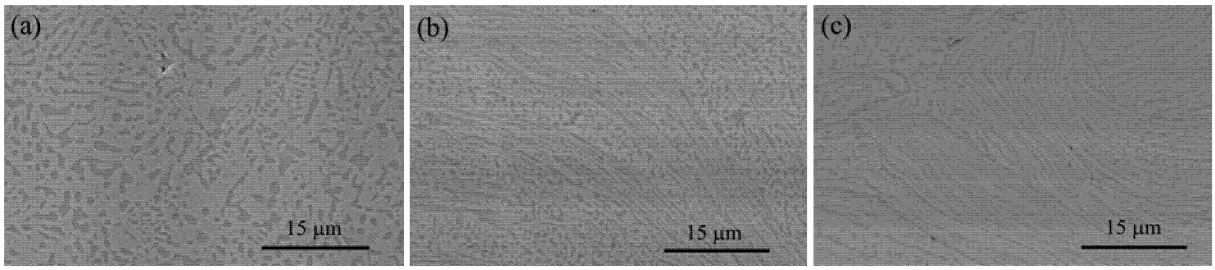

Fig.8: Cross sections of CoNiCrAlY samples obtained by SPS under different cryomilling and sintering conditions: (a) as-received powders (T_D=1000 °C), powders cryomilled at (b) t_{CR}=3h, CR=30 (T_D=850 °C), (c) t_{CR}=12h, CR=30 (T_D=900 °C).

These observations can be justified on the basis of the characteristics of the differently cryomilled powders subjected to SPS. Indeed, the two diverse microstructures identified within the same sample in Fig. 8(b) can be likely associated to the bimodal distribution observed when examining powders cryomilled for 3h at CR=30 (cf. Fig. 4(b). Thus, during SPS, powders belonging to the class with morphological and microstructural characteristics similar to the as-received material, i.e. the relatively smaller and regular particles shown in Fig. 4(b) when t_{CR}=3h at CR=30, generate the "classical" two-phases microstructure, as for the case of as-received powders. On the other hand, the second class of particles displaying a strongly modified morphology as an indication of the more intense treatment received, gives rise to the formation of the new sub-micrometer structure. These features are confirmed when examining the CoNiCrAlY sample obtained from the 12h cryomilled powders, which display more uniform characteristics (cf. Fig. 4(b)). Correspondingly, the finer microstructure tends to involve the entire bulk sample (cf. Fig. 8(c)).

To check if cryomilling would be beneficial towards the oxidation properties of CoNiCrAlY alloy, SPSed samples are exposed for 20 h to air at 1100 °C. The SEM image related to the cross section of an oxidized sample obtained by SPS when starting from standard powders is shown in Fig. 9(a) along with the corresponding EDS microanalysis result. An oxide layer 2-3 μm thick, mainly consisting of Al_2O_3, is formed on the sample surface. As reported in Fig. 9(b), XRD analyses performed on the surface of oxidized samples reveal the presence of other oxides, specifically Cr_2O_3 and spinel-like compounds (ex. $NiCr_2O_4$), other than α-Al_2O_3. It should be noted that, while the formation of the slow-growing oxides alumina and chromia has to be sustained to prevent internal oxidation of the alloy (Young, 2008), the presence of mixed oxides like spinels should be avoided, as they grow too fast to produce a protective scale. It should be noted that the γ/γ' and β peaks appearing on XRD patterns reported in Fig. 9(b) are due to the penetration of x-rays beyond the oxide layer, whose thickness is relatively low. More important, XRD peaks of Cr- and spinel-type-oxides, clearly detected when starting from unmilled powders, decrease in their intensity when sintering is preceded by the cryomilling step and no traces of them are found when oxidizing products obtained from severely milled powders (CR=30, t_{CR}=12 h).

It should be noted that the formation of α-Al_2O_3 is thermodynamically favoured as compared to the competing oxides mentioned above (Barin, 1989). Thus, when CoNiCrAlY samples are inizially exposed to the oxidizing environment at high temperature, Al is the first element that tends to be preferentially oxidized. However, the resulting incipient alumina layer will be not sufficient to guarantee material protection from the oxidation progress. Consequently, the formation of less protective mixed oxides like $NiCr_2O_4$ is possible, unless the amount of Al consumed on sample surface is rapidly replaced.

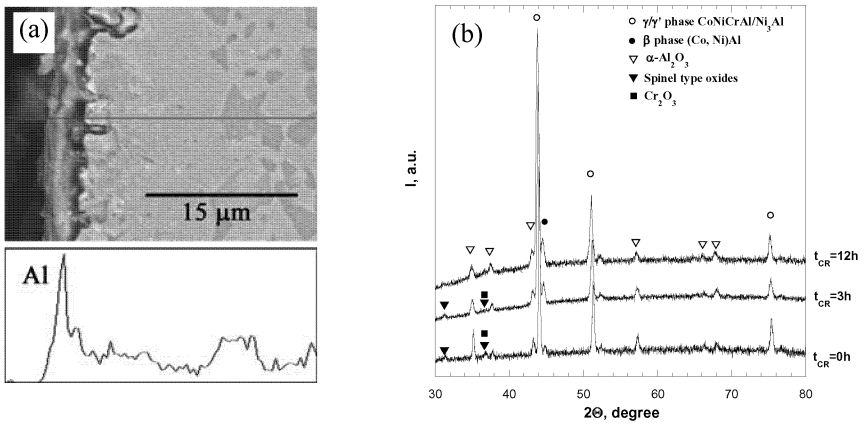

Fig.9: Characterization of oxidized bulk samples: (a) SEM image and corresponding Al line scan when starting from unmilled powder, (b) XRD patterns as a function of cryomilling time (CR=30).

The behaviour discussed above can be associated to the presence of the region about 15 μm thick, in the oxidized sample shown in Fig. 9, located adjacently to the oxide layer, where the β (darker) phase, rich in Al, almost disappears. This finding is consistent with previous observations reported in the literature on this subject (Tang et al., 2004). Indeed, the appearance of the β depletion zone near to the oxide scale is directly caused by Al

consumption in the sample surface after its oxidation. Consequently, the establishment of an Al gradient within the sample promotes the diffusion of this element towards material surface, thus gradually lowering the Al content in sample region approaching the oxide layer. Fig. 10 shows that the extension of the β phase depletion zone clearly decreases as the cryomilling intensity increases. Thus, at least under the experimental conditions investigated in this work, the superficial oxide layer formed on CoNiCrAlY samples exhibited a more protective character after the cryogenic treatment.
Indeed, a relatively smaller amount of Al to be oxidized is correspondingly required at the sample surface, thus indicating that the initially formed oxide layer provides a diffusion barrier to oxygen able to limit the progress of oxidation phenomena. This finding is consistent with the lower amount of spinel-type oxides decteted by XRD on the oxidized cryomilled systems (cf. Fig. 9b).

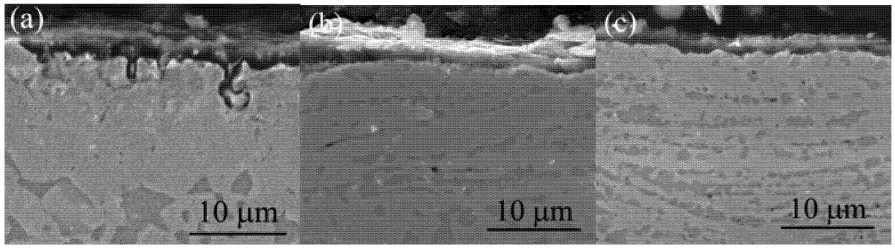

Fig.10: Cross sections of oxidized CoNiCrAlY samples obtained by SPS as a function of cryomilling time (CR=30): (a) t_{CR}=0h, (b) t_{CR}=3h, (c) t_{CR}=12h.

The observed behaviour can be justified on the basis of the microstructure refinement in product metal matrix (cf. Fig. 8) as well as the formation of nanosized oxide dispersoids induced by the cryomilling treatment. Both of these features likely play a relevant role during the initial oxidation stage, when the formation of a continuous protective layer of α-Al_2O_3 has to be favoured, while correspondingly avoiding that of undesired mixed oxides. For the quick replacement of the Al originally present on sample surface after its oxidation, a sufficiently high and continuous diffusion of this element through the CoNiCrAlY matrix has to be guaranteed. In this regards, microstructure refinement enhances the transport of an element across a metallic alloy because its diffusivity increases when decreasing grain size (Tang et al., 2004). Thus, the results obtained in the present study indicate that as the microstructure induced by cryomilling becomes finer, the Al diffusion rate increases and the condition to rapidly produce a dense and uniform alumina scale is satisfied. Apparently, this condition is not completely satisfied when using standard un-milled powders and the formation of other undesired oxides in the external scale becomes significant.
Another important role in the direction of improving the oxidation resistance of CoNiCrAlY alloys is played by the Al_2O_3 nanodispersions formed during cryomilling, that act as seeds for α-Al_2O_3 growth (Young, 2008) thus accelerating the selective formation of the protective scale.

4. CONCLUDING REMARKS

The influence of an attrition milling treatment conducted in liquid N_2 on Co-32Ni-21Cr-8Al-0.5Y (wt.%) powders characteristics, with particular emphasis on their spark plasma sintering behavior, is systematically investigated in this work. The most important changes evidenced when increasing either the cryomilling time or the charge ratio are powder flattening, particles size increase, grain size decrease, and formation of oxide dispersoids.
In addition, when powders are cryomilled at CR=30 up to 3h, a gradual increase in their sintering ability is observed as indicated by the corresponding decrease of the optimal sintering temperature to achieve the complete alloy consolidation from 1000 °C (as-received powders) to 850 °C. On the other hand, when cryomilling is prolonged to 12 h, less favorable sintering conditions (900 °C) are encountered. In any case, SPSed product microstructure becomes progressively finer with cryomilling. In particular, under the most critical milling conditions applied in this work, the γ (CoNiCrAl)/γ'(Ni_3Al) + β ((Co, Ni)Al) phases are finely distributed throughout the whole bulk sample at a sub-micrometric level.

The oxidation behavior exhibited by consolidated products when exposed to air at high temperature is strictly related to previous evidences. In fact, grain size refinement and/or the presence of oxide dispersoids during cryomilling promote the preferential formation of a continuous and dense layer of α-Al_2O_3 while the presence of less protective mixed oxides (spinels) is inhibited. This conclusion is supported by the minor Al depletion from the bulk of the alloy in cryomilled systems as compared to that observed in standard CoNiCrAlY.
Although the real benefits deriving from the cryomilling treatment can be verified only after powders deposition to produce the bond coat in a complete TBC, the preliminary use of the SPS method for rapidly preparing a set of fully dense specimens to be tested is very efficient and promising in view of extending the service life of gas-turbine components under the encountered oxidation conditions and/or increasing the corresponding operating temperature.

5. ACKNOWLEDGEMENTS

The financial support for this work by MIUR under the FIRB-2005 "Idee Progettuali" project (Contract number RBIP06X7F4) is gratefully acknowledged. The authors also thank Giovanni Bonanomi (Leco S.r.l., Italy), for oxygen content measurements.

6. REFERENCES

Ajdelsztajn L., Picas J.A., Kim G.E., Bastian F.L., Schoenung J., Provenzano V., 2002, Oxidation behavior of HVOF sprayed nanocrystalline NiCrAlY powder, Mat. Sci. Eng. A 338, 33-43.

Barin I., 1989, Thermochemical data of pure substances. Wiley-VHC, New York.

Langford J.I. and Wilson A.J.C., 1978, Scherrer after Sixty Years: A Survey and Some New Results in the Determination of Crystallite Size, J. Appl. Crystallogr. 11, 102-113.

Lavernia E.J., Han B.Q. and Schoenung J.M., 2008, Cryomilled nanostructured materials: Processing and properties, Mater. Sci. Eng. A 493(1-2), 207-214.

Locci A.M., Orrù R., Cao G., Munir Z.A., 2006, Simultaneous Spark Plasma Synthesis and Densification of TiC-TiB_2 Composites, J. Am. Ceram. Soc. 89, 848-855.

Ma K., Schoenung J.M., 2010, Influence of cryomilling on the microstructural features in HVOF-sprayed NiCrAlY bond coats for thermal barrier coatings: Creation of a homogeneous distribution of nanoscale dispersoids, Phil. Mag. Lett. 90, 739-751.

Oquab D., Estournesand C., Monceau D., 2007, Oxidation resistant aluminized MCrAlY coating prepared by Spark Plasma Sintering (SPS), Adv. Eng. Mater. 9, 413-417.

Orrù R., Licheri R., Locci A.M., Cincotti A. and Cao G., 2009, Consolidation/synthesis of materials by electric current activated/assisted sintering, Mater. Sci. Eng. R 63(4-6), 127-287.

Ratel N., Monceau D., Estournès C., Oquab D., 2010, Reactivity and microstructure evolution of a CoNiCrAlY/Talc cermet prepared by Spark Plasma Sintering, Surf. Coat. Tech. 205, 1183-1188.

Sahoo P., Carr T., Martin R. and Dinh F., 1998, Thermal spray manufacturing issues in coating IGT hot section components, J. Therm. Spray Technol. 7(4), 481-483.

Song J., Ma K., Zhang L., Schoenung J.M., 2010, Simultaneous synthesis by spark plasma sintering of a thermal barrier coating system with a NiCrAlY bond coat, Surf. Coat. Tech. 205, 1241-1244.

Suryanarayana C., 2001, Mechanical alloying and milling, Prog. Mater. Sci. 46, 1-184.

Tang F., Ajdelsztajn L. and Schoenung J.M., 2004, Influence of Cryomilling on the of the Oxide Scales Formed on HVOF CoNiCrAlY Coatings, Oxid. Met. 61(314), 219-238.

Young D.J., 2008, High Temperature Oxidation and Corrosion of Metals, Elsevier Science Publishing Company.

Witkin D.B. and Lavernia E.J., 2006, Synthesis and mechanical behavior of nanostructured materials via cryomilling, Prog. Mater. Sci. 51(1), 1-60.